

# Disparities in the impact of urban heat island effect on particulate pollutants at different pollution stages - A case study of the “2 + 36” cities

Chang Yinghui <sup>a</sup>, Guo Xiaomin <sup>b,\*</sup>

<sup>a</sup> College of Geography and Environmental Science, Henan University, Kaifeng 475004, China

<sup>b</sup> Institute of Finance and Economics, School of Urban and Regional Science, Shanghai University of Finance and Economics, Shanghai 200433, China



## ARTICLE INFO

### Keywords:

PM pollution  
SUHII  
LST  
Piecewise linear regression  
GTWR  
“2 + 36” cities

## ABSTRACT

Urban heat island (UHI) and atmospheric pollution are critical ecological challenges in urban areas. China's air quality presents a stage-specific “polluting first and cleaning up later” model. However, the differential impact of UHI on particulate matter (PM) pollution across various stages remains unclear. This study utilizes land surface temperature (LST) data between 2000 and 2021 to calculate the surface urban heat island intensity (SUHII) across the “2 + 36” cities, a key pollution prevention and control area. The inflection points of PM pollution in each city were identified through piecewise linear regression, dividing the study period into distinct pollution stage. The geographical and temporal weighted regression (GTWR) model was employed to analyze the varying impacts of SUHII on PM pollution across different stages. The result indicate that UHI persisted significantly during the study period. The impact of SUHII on PM pollution exhibits pronounced temporal and regional characteristics, with an increasing influence of Nighttime SUHII (N\_SUHII) on pollution. This finding highlights a crucial entry point for future pollution control measures. Moreover, under the influence of SUHII, ecological factors such as enhanced vegetation index and precipitation may paradoxically exacerbate PM pollution at certain times. These findings reveal the multifaceted causes and dynamics of urban PM pollution in developing countries, validate the necessity of implementing targeted management measures in the context of future climate change, and are important for the formulation of strategies to promote sustainable urban development.

## 1. Introduction

In recent decades, global urban climates have undergone significant changes (Liu et al., 2021). The rapid urbanization process has caused more and more natural landscapes to be replaced by artificial surfaces, which has a significant negative impact on the urban ecological environment (Grimm et al., 2008). For instance, urban particulate matter (PM) pollution and the urban heat island (UHI) are typical byproducts of rapid urbanization (Lin et al., 2020). UHI refers to the phenomenon where urban areas exhibit higher surface and atmospheric temperatures than surrounding suburban areas (Voogt and Oke, 2003), affecting urban climate (Mackey et al., 2012), air conditions (Lai and Cheng, 2009) and human health (Estoque et al., 2020a, 2020b), thereby significantly reducing residents' quality of life. The increase in land surface temperature (LST) exacerbates the thermal stress on urban residents, especially during summer. To

\* Corresponding author.

mitigate thermal discomfort during hot summers or cold winters, substantial energy consumption for cooling or heating is required, leading to a significant rise in energy consumption (Kolokotroni et al., 2006). Simultaneously, emissions from industrial production, residential activities, and transportation further aggravate the adverse effects on human health and climate change (Qi et al., 2017). Numerous studies have demonstrated that the intensity, frequency and duration of urban heatwaves are increasing due to global climate change (Meehl and Tebaldi, 2004), and surface urban heat island (SUHI) are expected to intensify in most cities (Liu et al., 2022). The deterioration of the urban thermal environment not only threatens human health, but also exacerbates energy consumption and air pollution (Estoque et al., 2020a, 2020b; Santamouris, 2020), posing significant challenges to urban livability and sustainable development (Chen et al., 2024a). Therefore, in the current context, it is essential to investigate how SUHI impacts urban PM concentrations, considering various other socio-ecological factors.

In recent years, research on the interrelationship between SUHI and air quality has made significant progress. In a study of Paris, Sarrat (Sarrat et al., 2006) first revealed the substantial impact of daytime and nighttime SUHI on regional air pollution, laying the foundation for subsequent research. Generally, SUHI significantly influences the concentration and distribution of atmospheric particulate matter in cities, with the effect being modulated by city scale, climatic conditions, and seasonal variations (Ngarambe et al., 2021). Firstly, SUHI can affect the diffusion and deposition of PM pollutants by altering local climatic conditions, especially by increasing LST. Since SUHI typically enhances the vertical mixing layer thickness of the city, it leads to pollutant accumulation in the lower atmosphere, worsening air quality, particularly in large cities like Beijing (Yang et al., 2021). While air circulation usually aids in dispersing atmospheric particulate matter, the urban atmospheric boundary layer and inversion layers associated with SUHI can hinder pollutant migration and transmission. Especially during temperature inversions, pollutants from suburban areas may migrate back into urban areas, further deteriorating air quality.

In addition, air pollution can exacerbate SUHI. Specifically, atmospheric particulate pollutants can reduce the amount of solar radiation reaching the surface by absorbing and scattering it, thereby altering the surface energy balance (Luo et al., 2019). The weakening of this radiative cooling effect increases local temperature, further intensifying SUHI. Studies have shown that PM<sub>2.5</sub> and PM<sub>10</sub> not only change the thermodynamic properties of cities by absorbing and scattering solar radiation (Zhang et al., 2014; Wang et al., 2014), but also affect cloud formation and properties by changing atmospheric optical properties, further influencing the local climate (Tie et al., 2017). Complicating matters further, significant seasonal differences exist between SUHI and air pollution,

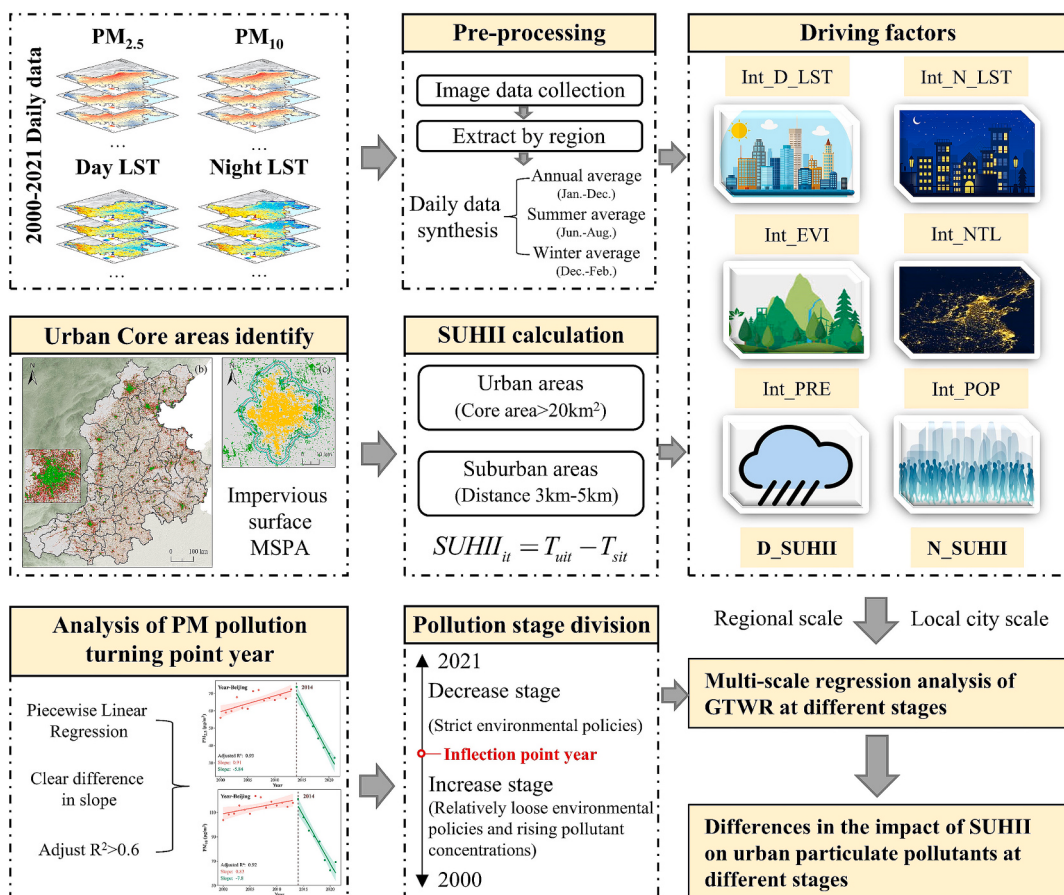


Fig. 1. Research framework diagram.

especially in northern China, which experiences four distinct seasons (Wang et al., 2018). While, at present, there is still a lack of systematic research in this area. Therefore, a comparative study of the differences in the effects of SUHI on air pollution from different seasons is necessary, especially in winter and summer.

The “2 + 36” cities constitute one of China’s key air pollution prevention and control regions, plagued by severe and complex air pollution issues. China experienced an extreme haze event in 2013, with this region being the epicenter of pollution (Tian et al., 2014). On a single day during this event, Beijing’s PM<sub>2.5</sub> concentration exceeded the health standard set by the World Health Organization (WHO) by more than 40 times, severely impacting residents’ health and daily life (Martin Patience, 2013). Since the implementation of the “Action Plan for Prevention and Control of Air Pollution”, significant progress has been made in air pollution in this region, with a marked reduction in heavy pollution episodes (Geng et al., 2019). However, its air quality remains far below WHO’s recommended standards, with occasional pollution rebounds (Zeng et al., 2019). This region is a typical area that reflects pollution control and changes in pollution characteristics at different phases.

This apparent phasing reflects differences in human activity levels and policy contexts at different times, which may lead to changes in atmospheric particulate pollution mechanisms. Compared with the previous “extensive” development model, the impact of SUHI on urban air quality may have undergone significant changes in recent years under stricter pollution control measures. However, most of the previous studies have analyzed the pollution mechanism as a whole based on a single period only, and less quantitative methods have been used to identify pollution inflection points and classify different stages of particulate matter pollution, in order to better clarify the impact of human activities and policies on pollutants. Therefore, in the context of the increasing SUHI, it is crucial to further understand the formation mechanism of particulate pollutants, so as to formulate more comprehensive and targeted mitigation strategies, and explore the differences in the impact of SUHI and socio-ecological factors on urban PM pollutants at different stages (Zhao and Wang, 2022). The main purposes of this study are to: (1) Reveal the temporal and spatial evolution of LST and PM pollutants (PM<sub>2.5</sub> and PM<sub>10</sub>) in the “2 + 36” cities at different scales. (2) Calculate surface urban heat island intensity (SUHII) based on LST data and explore the correlation between SUHII and PM pollution across different seasons. (3) Use piecewise linear regression to identify the inflection points of PM<sub>2.5</sub> and PM<sub>10</sub> pollution in each city separately and divide different pollution stages. (4) Analyze the impact of SUHII and its influential socio-ecological factors on PM pollution across different pollution stages at both regional and city scales. Fig. 1 illustrates the primary research framework of this study.

## 2. Materials and methods

### 2.1. Overview of the study area

The “2 + 36” cities (33°03' ~ 41°36'N, 110°22' ~ 119°50'E) are primarily situated in the North China Plain, covering about 37.07 × 10<sup>4</sup> km<sup>2</sup>, which is 3.86 % of China’s total land area. The region is bordered by the Taihang and Yanshan mountains to the west and north, and the Shandong hills to the east, featuring a warm-temperate sub-humid monsoon climate with four distinct seasons (Fig. 2). The “2 + 36” cities are a core part of the Beijing-Tianjin-Hebei urban agglomeration, a significant hub for northern China’s economic growth. In 2021, this regional accounted for 16.96 % of China’s GDP and had a population of 272 million, about 19.27 % of the nation’s total. Over recent decades, rapid urbanization and industrialization have led to severe environmental challenges, including complex air pollution, consistent with the environmental Kuznets curve phenomenon (Chen et al., 2013; Chen et al., 2024a). In 2023, the “Action Plan for Continuous Improvement of Air Quality” expanded the original “2 + 26” cities to “2 + 36” cities, eliminating gaps between Beijing-Tianjin-Hebei area and the Yangtze River Delta, thus forming a more unified air pollution control region.

Note: 1-Beijing, 2-Tianjin, 3-Shijiazhuang, 4-Tangshan, 5-Qinhuangdao, 6-Handan, 7-Xingtai, 8-Baoding, 9-Cangzhou, 10-

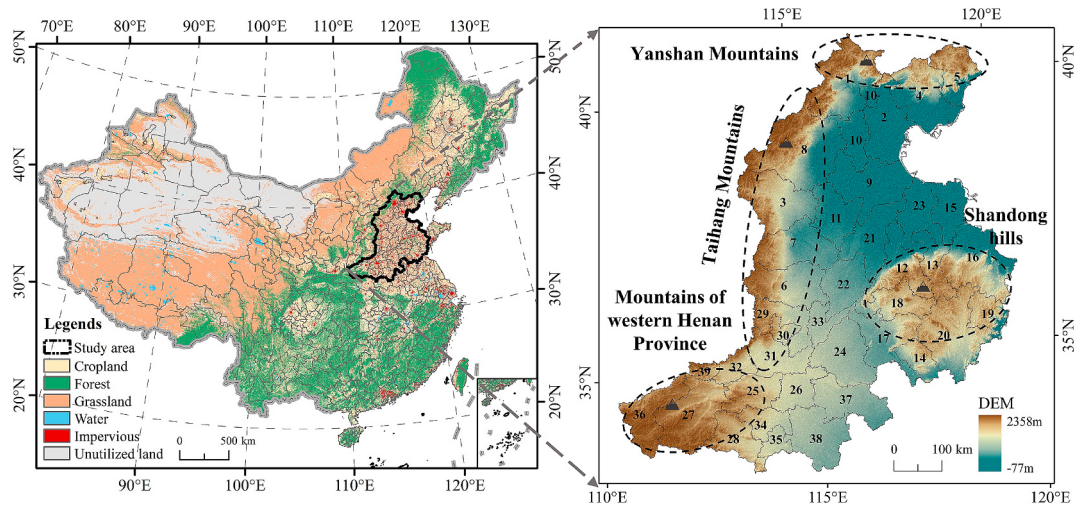


Fig. 2. Map of study area.

Langfang, 11-Hengshui, 12-Jinan, 13-Zibo, 14-Zaozhuang, 15-Dongying, 16-Weifang, 17-Jining, 18-Taian, 19-Rizhao, 20-Linyi, 21-Dezhou, 22-Liaocheng, 23-Binzhou, 24-Heze, 25-Zhengzhou, 26-Kaifeng, 27-Luoyang, 28-Pingdingshan, 29-Anyang, 30-Hebi, 31-Xinxiang, 32-Jiaozuo, 33-Puyang, 34-Xuchang, 35-Luohe, 36-Sanmenxia, 37-Shangqiu, 38-Zhoukou, 39-Jiyuan. Produced on the basis of the standard Chinese map of the Ministry of Natural Resources, Standard Map Service Website Audit No. GS(2019)1822, with the boundaries of the base map unchanged.

## 2.2. Data source

This study mainly involves three types of data: PM pollution data, LST data and other socio-ecological data, as detailed in [Table 1](#). To accurately reflect the urban heat situation, we selected the Aqua satellite product in the TRIMS LST dataset, referencing previous research experience ([Zhao et al., 2024](#)). The Aqua satellite's transit time is particularly suitable for studying SUHI. The original value (DN) in the dataset was converted to LST by the following equation:

$$T_i = DN \times 0.01 - 273.15 \quad (1)$$

where  $T_i$  (°C) represents the surface temperature of each pixel;  $DN$  is the brightness value. Given the large data volume, processing was done using Arcpy toolkit in Python 2.7.

The PM pollution data and LST data were processed by R software to obtain monthly, seasonal and annual averages. Because the PM dataset used in this study was obtained by combining big data production from ground-based observations, atmospheric reanalysis, and emission inventories, the PM data in this study are not divided into day and night. In addition, combined with climatic characteristics of the “2 + 36” cities, summer range of this study was defined as June–August and winter was December–February.

For further investigate the impact of SUHI on PM pollution, based on the characteristics of the urban environment and previous research experience ([Chen et al., 2024a, 2024b](#)), we also selected six other socio-ecological factors as covariates, including daytime LST (D\_LST), nighttime LST (N\_LST), enhanced vegetation index (EVI), precipitation (PRE), population density (POP), and nighttime light (NTL). Among them, EVI, PRE, POP and NTL were processed based on Google Earth Engine (GEE). In addition, the relationship between SUHII and PM pollution explored in this study is only for clear-sky conditions, since SUHII is calculated from LST, which is derived from thermal infrared remote sensing products.

## 2.3. Research methods

### 2.3.1. Theil-Sen estimator and Mann-Kendall test

Given the extended study period, the Theil-Sen estimator and Mann-Kendall test (TS-MK) were employed to analyze PM pollution and LST trends. The Theil-Sen estimator provides a robust, non-parametric slope estimation, maintaining reliability even with outliers or non-normal data distributions ([Cao et al., 2022; Cao et al., 2023](#)). The specific calculation formula is as follows:

$$\text{Trend} = \text{median} \frac{x_j - x_i}{j - i} (1 < i < j < n) \quad (2)$$

**Table 1**

Data sources involved in the study.

Data type	Data name	Year	Spatial resolution	Temporal resolution	Data sources
PM <sub>2.5</sub>	CHAP	2000–2021	1 km	Daily	<a href="#">Wei and Li (2023a)</a> <a href="https://doi.org/10.5281/zenodo.3539349">https://doi.org/10.5281/zenodo.3539349</a>
PM <sub>10</sub>	CHAP	2000–2021	1 km	Daily	<a href="#">Wei and Li (2023b)</a> <a href="https://doi.org/10.5281/zenodo.3752465">https://doi.org/10.5281/zenodo.3752465</a>
Land surface temperature (LST)	TRIMS LST	2000–2021	1 km	Daily	<a href="#">Zhou et al. (2021)</a> <a href="https://doi.org/10.11888/Meteoro_tpdc.271252">https://doi.org/10.11888/Meteoro_tpdc.271252</a>
Impervious surface map	The 30m annual land cover dataset	2000–2021	30 m	Annually	<a href="#">Yang and Huang (2021)</a> <a href="https://doi.org/10.5194/esd-13-3907-2021">https://doi.org/10.5194/esd-13-3907-2021</a>
Enhanced vegetation indices (EVI)	MOD13Q1	2000–2021	250 m	16 days	<a href="#">NASA EOS/MODIS</a> <a href="https://ladsweb.modaps.eosdis.nasa.gov/">https://ladsweb.modaps.eosdis.nasa.gov/</a>
Precipitation (PRE)	CHIRPS	2000–2021	0.05°	Daily	<a href="#">Funk et al. (2015)</a> <a href="https://doi.org/10.1038/sdata.2015.66">https://doi.org/10.1038/sdata.2015.66</a>
Population density (POP)	Landscan population density datasets	2000–2021	1 km	Annually	<a href="#">Oak Ridge National Laboratory</a> <a href="https://landscan.ornl.gov/">https://landscan.ornl.gov/</a>
Night light index (NTL)	DMSP-OLS-like data	2000–2021	1 km	Annually	<a href="#">Harward dataverse</a> <a href="https://doi.org/10.7910/DVN/GIYGJU">https://doi.org/10.7910/DVN/GIYGJU</a>

where  $Trend$  is the PM or LST trend,  $x_i, x_j$  are annual averages,  $n$  is the time series length. When  $Trend > 0$ , indicates an increase trend.

The Mann-Kendall test is a non-parametric statistical method for detecting whether there is a monotonic upward or downward trend in the time series and judging the significance of the trend (Zhang et al., 2022). The calculation formula is as follows:

$$Z_{MK} = \begin{cases} \frac{S - 1}{\sqrt{var(S)}}, S > 0 \\ 0, S = 0 \\ \frac{S + 1}{\sqrt{var(S)}}, S < 0 \end{cases} \quad (3)$$

$$var(S) = \frac{n(n-1)(2n+5)}{18} \quad (4)$$

$$S = \sum_{i=1}^{n-1} \sum_{j=i+1}^n sgn(x_j - x_i) \quad (5)$$

$$sgn(x_j - x_i) = \begin{cases} 1, x_j - x_i > 0 \\ 0, x_j - x_i = 0 \\ -1, x_j - x_i < 0 \end{cases} \quad (6)$$

where  $Z_{mk}$  is the statistical test of a single sequence.  $S$  is calculated from the sequence raster data of PM or LST,  $var(S)$  is the variance of  $S$ ,  $sgn$  is the logistic discriminant function. In this study, a threshold of  $Z = 1.96$  was selected to determine significant changes.

The Theil-Sen method provides the slope estimation of the trend, while the Mann-Kendall method is used to test the significance of the trend. The combination of the two methods can comprehensively and scientifically analyze the changes of PM pollutants and LST in different seasons.

### 2.3.2. SUHII calculation

SUHII is directly dependent on LST measurements and is an expression of the difference between urban and suburban surface temperatures. SUHII represents the LST difference between urban and suburban areas (Peng et al., 2012). Using the data of land cover types in China (Yang and Huang, 2021), we extracted impervious surface within the “2 + 36” cities. Morphological Spatial Pattern Analysis (MSPA) was applied to analyze landscape patches, because it can effectively solve the problem of differences in impervious surface size, spatial distribution and connectivity (Yu et al., 2021). Therefore, based on ArcGIS 10.8 and Guidos, we took the impervious surface as the foreground, 1, 2 and 4 pixels were selected as the boundary widths for testing, and the area with the core area of more than  $20\text{km}^2$  was measured and extracted as urban area. In addition, we also created multiple buffers with an interval of 1 km based on the urban area, and define the buffer between 3 and 5 km as suburban area (Fig. 3). This method can effectively distinguish between urban and suburban areas, capture the difference of SUHI, and improve the accuracy of measurement (Zhou et al., 2015). Urban and suburban LST of each city is represented by the arithmetic mean of pixels in each region. The calculation formula is as follows:

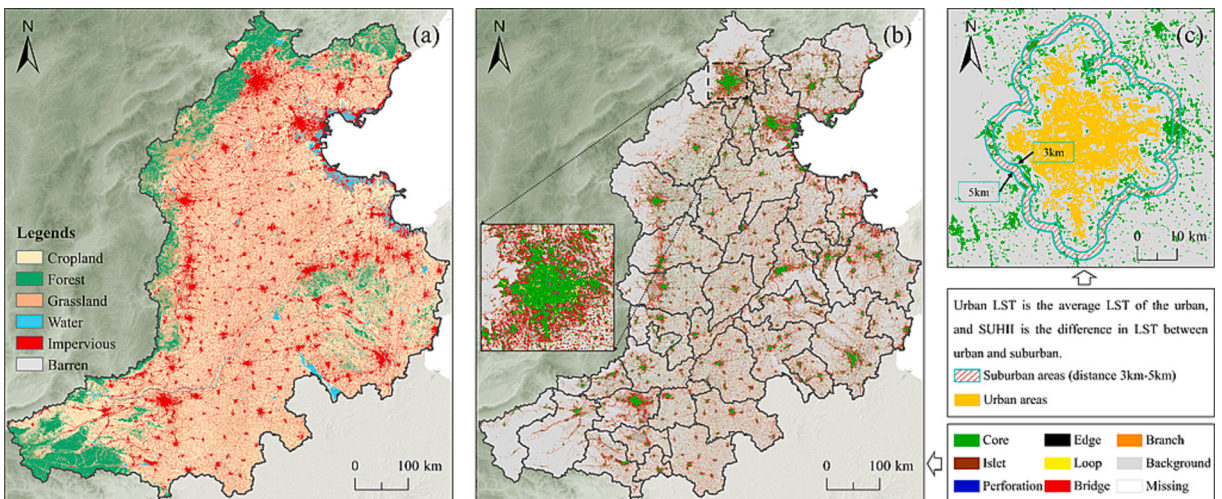


Fig. 3. MSPA methodology to identify urban and suburban areas.

$$SUHII_{it} = T_{uit} - T_{sit}$$
(7)

where  $SUHII_{it}$  is the SUHII of the  $i_{th}$  city in  $t$  period,  $T_{uit}$  represents the LST mean data of the urban area of the  $i_{th}$  city in  $t$  years,  $T_{sit}$  represents the LST mean data of the suburbs of the  $i_{th}$  city in  $t$  years.

### 2.3.3. PM pollution stage division

China's air pollution trends demonstrate an obvious characteristics of "polluting first and cleaning up later", reflecting different pollution mechanisms at various development stages (Li et al., 2023). By dividing the air quality development stages, this study aims to more accurately identify the changes in socio-ecological factors across different stages, enabling the formulation of targeted governance strategies.

In this study, the "2 + 36" cities were analyzed by the piecewise linear regression model. The dependent variables were the annual average, summer average, and winter average concentrations of  $PM_{2.5}$  and  $PM_{10}$ , while the independent variable was the year. This method can effectively extract the trend inflection points in long-term series data, addressing the limitations of ordinary linear regression, which may not accurately reflect changes in trends. It has been widely used in trend analysis (Chen et al., 2024b). The calculation formula is as follows:

$$Y = \begin{cases} \beta_1 t + \lambda_1, & t \leq \alpha \\ \beta_2 t + \lambda_2, & t > \alpha \end{cases} \quad (8)$$

where  $Y$  is the pollutant concentration,  $t$  is the year,  $\alpha$  is the inflection point of the detected time series,  $\beta$  is the slope before and after the inflection point, and  $\lambda$  is the intercept before and after the inflection point. These parameters are obtained by the least square method. Referring to the research of Chen et al. (Chen et al., 2024a) and considering real-world air pollution control efforts, the criteria for selecting the inflection point in this study are as follows: (1) There is a significant difference in the fitting slope before and after the inflection point. (2) Adjust  $R^2$  after piecewise regression is not less than 0.6. (3) Based on the reality of air pollution control, the number of inflection points is limited to 1, and it is limited to the mid-term selection of the research period. (4) The rounding method of the inflection point is selected as the upward rounding.

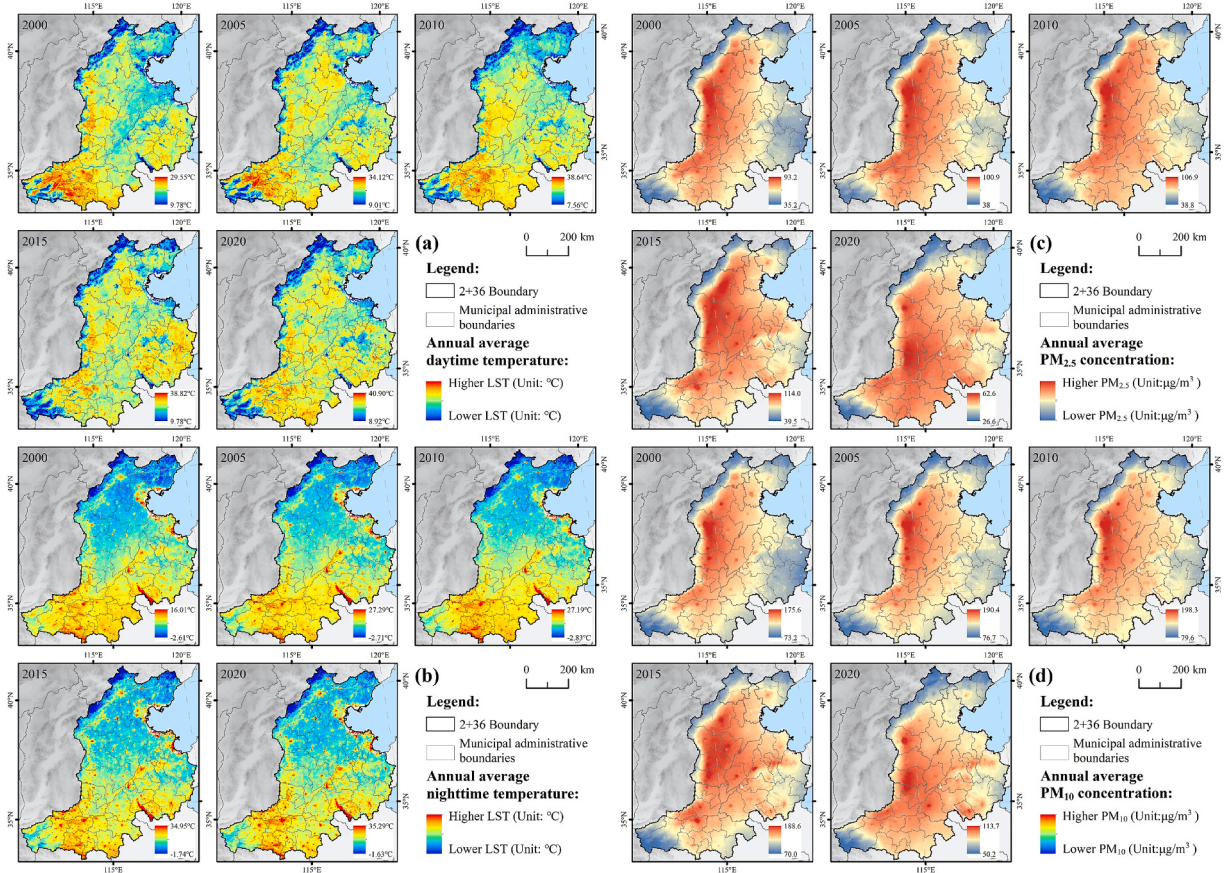


**Fig. 4.** Spatial distribution of daytime and nighttime LST and PM pollutants.

### 2.3.4. Geographical and temporal weighted regression (GTWR)

The traditional linear regression model is limited in its ability to capture the true spatial characteristics of regression parameters. To address this, the study employs the GTWR model, which quantifies the spatial heterogeneity of each influencing factor. Unlike the geographically weighted regression (GWR) model, GTWR incorporates the time factor, allowing for an accurate analysis of panel data on PM pollution concentrations over long time series. This approach resolves issues of spatio-temporal non-stationarity and improves parameter estimation (Wu et al., 2021a, 2021b). The calculation formula is as follows:

$$w_i = \beta_0(u_i, v_i, t_i) + \sum_{k=1}^p \beta_k(u_i, v_i, t_i)m_{ik} + \varepsilon_i, i = 1, 2, 3, \dots, n \quad (9)$$

where  $w_i$  is the explained variable, representing the concentration of particulate pollutants in each city.  $m_{ik}$  is the  $k$ th explanatory variable for the  $i$ th city. Since this study focuses on exploring the impact of SUHII on PM pollution, the six other socio-ecological factor explanatory variables are the interaction terms generated by them respectively with SUHII.  $(u_i, v_i, t_i)$  is the spatio-temporal coordinates of city  $i$ .  $p$  is the number of influencing factors.  $\beta_k$  is the estimated coefficients of explanatory variables.  $\beta_0$  is the intercept term.  $\varepsilon_i$  is the random perturbation term.

The core of GTWR lies in the selection of spatial weight function, and the spatial correlation of data is constructed through a spatial weight matrix. This study applied the spatial-temporal weight function and spatial-temporal distance based on the Gaussian function method proposed by Huang (Huang et al., 2008), which integrates spatial and temporal two-dimensional information.

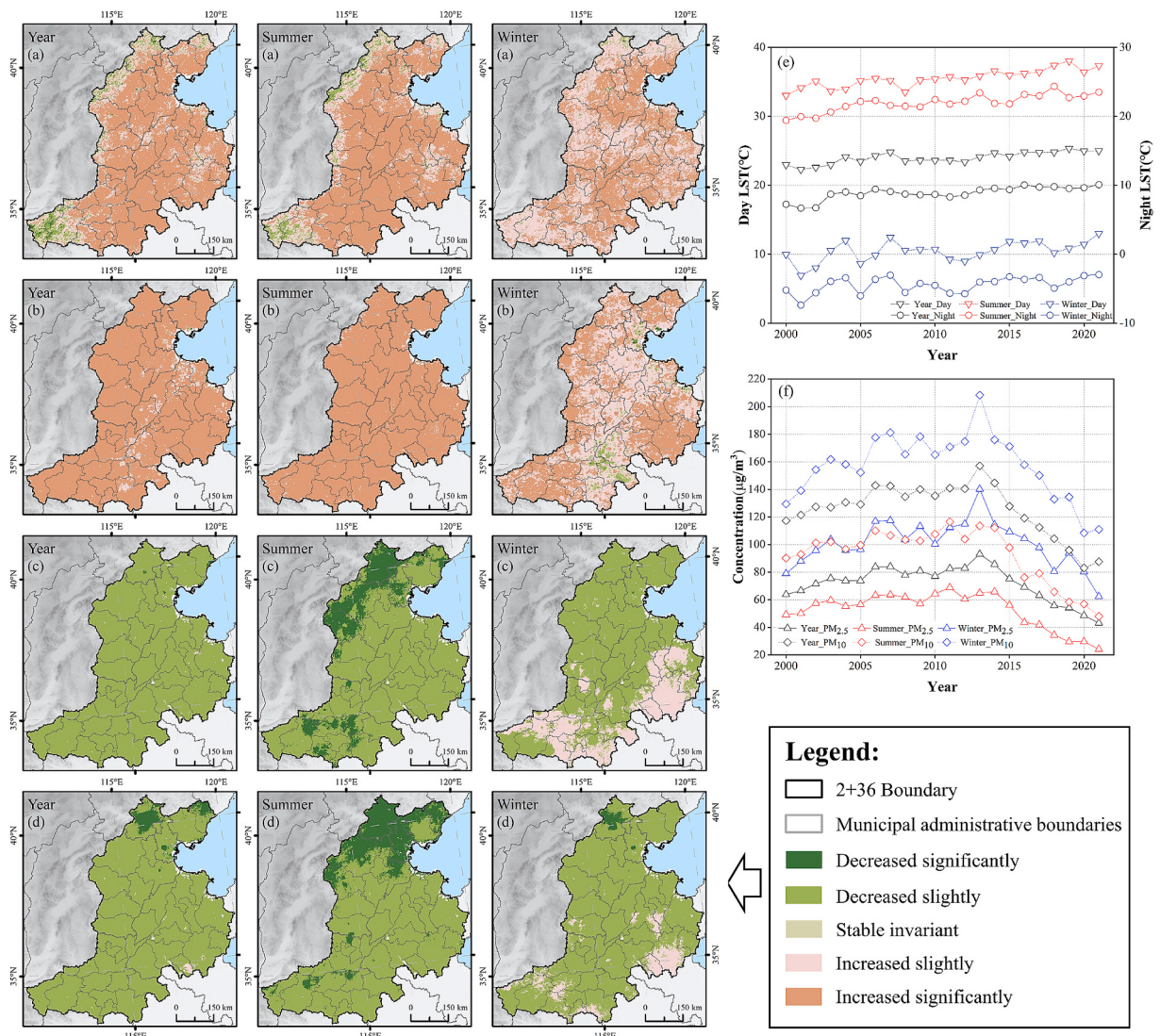


**Fig. 5.** Daytime and nighttime LST and PM pollution trends.

### 3. Results

#### 3.1. Evolution characteristics of LST and SUHII

Due to the long time period of the study, in order to show the evolution of LST and PM pollutants spatially, five breakpoint years, 2000, 2005, 2010, 2015 and 2020, are used in this study. During the study period, the LST in daytime and nighttime across the “2 + 36” cities exhibited significant spatial heterogeneity (Fig. 4 (a)-(b)). Overall, urban areas with dense population and transportation are the main hotspot distribution areas, while the regional cold spot distribution areas are mainly located in mountainous areas. Notably, due to the difference in thermal properties between land and sea, the temperature along the Bohai Bay coast was lower during the day and relatively higher at night. Contrary to nighttime, the daytime average LST did not consistently follow latitude changes, potentially due to differences in water vapor exchange across various topographic areas and varying heat capacity and conduction related to different land use types (Giovannini et al., 2020).

To further investigate trends over time, we applied the TS-MK to access changes in annual, summer and winter averages of daytime and nighttime LST at the pixel scale (Fig. 5 a-b). Fig. 5a revealed that although D\_LST generally increased, local differences were evident. The N\_LST trend was more complex, with annual and summer averages primarily showing an increasing trend. Almost all patches in summer exhibited significant increases, while some coastal and southern areas experienced decreases in winter (Fig. 5b).

After horizontally comparing the spatial distribution and changes in daytime and nighttime LST, we also analyzed its temporal changes at the regional scale, with the average LST line chart for each period shown in Fig. 5e. Over the long-term (2000–2021), the region’s LST exhibited a noticeable fluctuating upward trend, with N\_LST fluctuations being more pronounced than D\_LST. This difference may be due to the absence of solar radiation at night, making LST more susceptible to ground properties, atmospheric conditions, and human activities. The fluctuation range in winter is greater than summer, which is related to the weak solar radiation and complex meteorological phenomena in winter. The existence of snow and ice will also lead to greater fluctuation range.

To examine the temperature relationship between urban and suburban areas, we calculated the temperature differences under six scenarios: summer daytime, summer nighttime, winter daytime, winter nighttime, annual daytime and annual nighttime (Fig. 6). The results indicate that, except for winter daytime, urban area consistently had higher temperatures than suburban areas, demonstrating significant SUHI effects in the “2 + 36” cities. Nighttime SUHII (N\_SUHII) increased significantly, while Daytime SUHII (D\_SUHII) was more complex. Overall, SUHII values were highest in summer and lowest in winter. Given the complexity of LST differences between urban and suburban areas, it is essential to explore how SUHII affects urban particulate matter pollution at different times.

#### 3.2. Relationship between SUHII and PM pollution

Given the distinct seasonal characteristics of SUHII in winter and summer, further investigating the relationship between LST and PM pollutants during these seasons is essential to better understand their interactions. Fig. 7 illustrates scatter plots of daytime and nighttime LST versus PM pollution and the results of correlation analysis in both urban and suburban areas during summer and winter. Except for the winter daytime LST and PM<sub>10</sub>, which did not pass the significance test, all other results showed a significant correlation

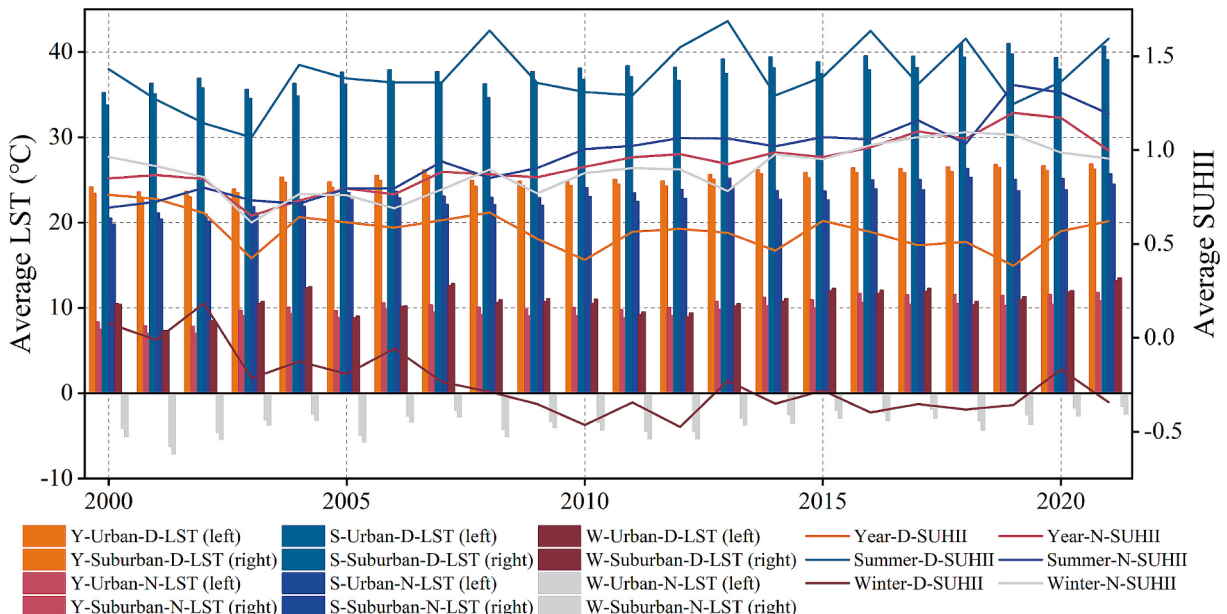


Fig. 6. LST comparison between urban and suburban areas and SUHII evolution.

( $p < 0.01$ ). In summer, a significant negative correlation was observed, indicating that as LST increased, PM pollution decreased markedly, both during the day and at night. This could be due to higher temperatures enhancing vertical atmospheric mixing, promoting the dispersion and dilution of PM pollutants (Jiang et al., 2021). However, during summer nights, the situation in urban and suburban areas is different, mainly in the following aspects: (1) The negative correlation between LST and  $\text{PM}_{2.5}$  in suburban areas ( $\beta = -0.339^{**}$ ) was stronger than that in urban areas ( $\beta = -0.319^{**}$ ), while the opposite was seen during the daytime. (2) The negative correlation between LST and  $\text{PM}_{10}$  in urban area ( $\beta = -0.333^{**}$ ) was stronger than suburban ( $\beta = -0.297^{**}$ ), with the opposite relationship observed during the day.

In winter, LST was positively correlated with both particulate pollutants, although the correlation was significantly weaker than in summer. This weaker correlation might result from reduced solar radiation in winter, which limits vertical atmospheric mixing and leads to pollutant accumulation (Zhu et al., 2018). As previously mentioned, SUHII was notably higher in summer compared to winter, and the correlation between LST and PM pollution differs between urban and suburban areas. These differences reflect the varying impacts of different land use types and SUHI on pollutant distribution. Therefore, it is scientifically sound and reasonable to explore the influence of SUHII on PM pollution by season, as well as by day and night. This approach allows for a more comprehensive understanding of how SUHI affects PM pollution dynamics.

### 3.3. Evolution characteristics and inflection point identification of PM pollution

Through the spatial distribution analysis of the five sections in typical years, 2000, 2005, 2010, 2015 and 2020, it is evident that  $\text{PM}_{2.5}$  and  $\text{PM}_{10}$  concentrations in the “2 + 36” cities exhibit pronounced spatial aggregation characteristics throughout the study period (Fig. 4 (c)-(d)). The main pollution areas are located in regions surrounded by mountains in the north and west and hills in the east, forming more evident point-strip aggregations. Notably, continuous strip pollution areas have emerged, particularly in Beijing-Baoding-Shijiazhuang-Xingtai, with  $\text{PM}_{10}$  pollution showing stronger point-source aggregation characteristics compared to  $\text{PM}_{2.5}$ . However, with the progressive implementation of pollution control measures, PM pollution concentrations have significantly decreased by 2020, with the peak pollution levels nearly halved compared to 2015. The regions surrounding Beijing have seen considerable improvement, and the focus of air pollution has shifted to the south and east.

The TS-MK test at the pixel scale was used to analyze trends in annual average, summer average, and winter average  $\text{PM}_{2.5}$  and  $\text{PM}_{10}$  concentrations (Fig. 5 c-d). Regardless of the period analyzed, the proportion of areas showing a decreasing trend in pollutant

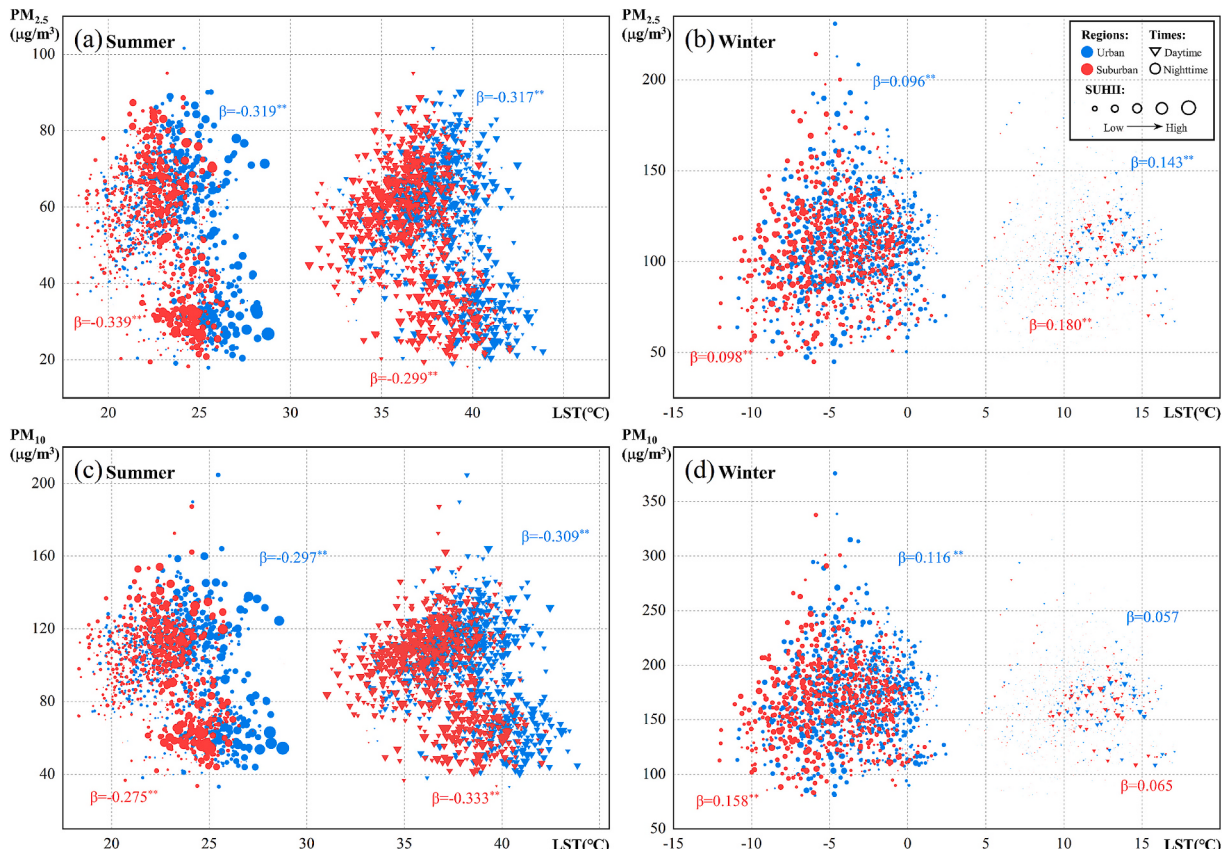
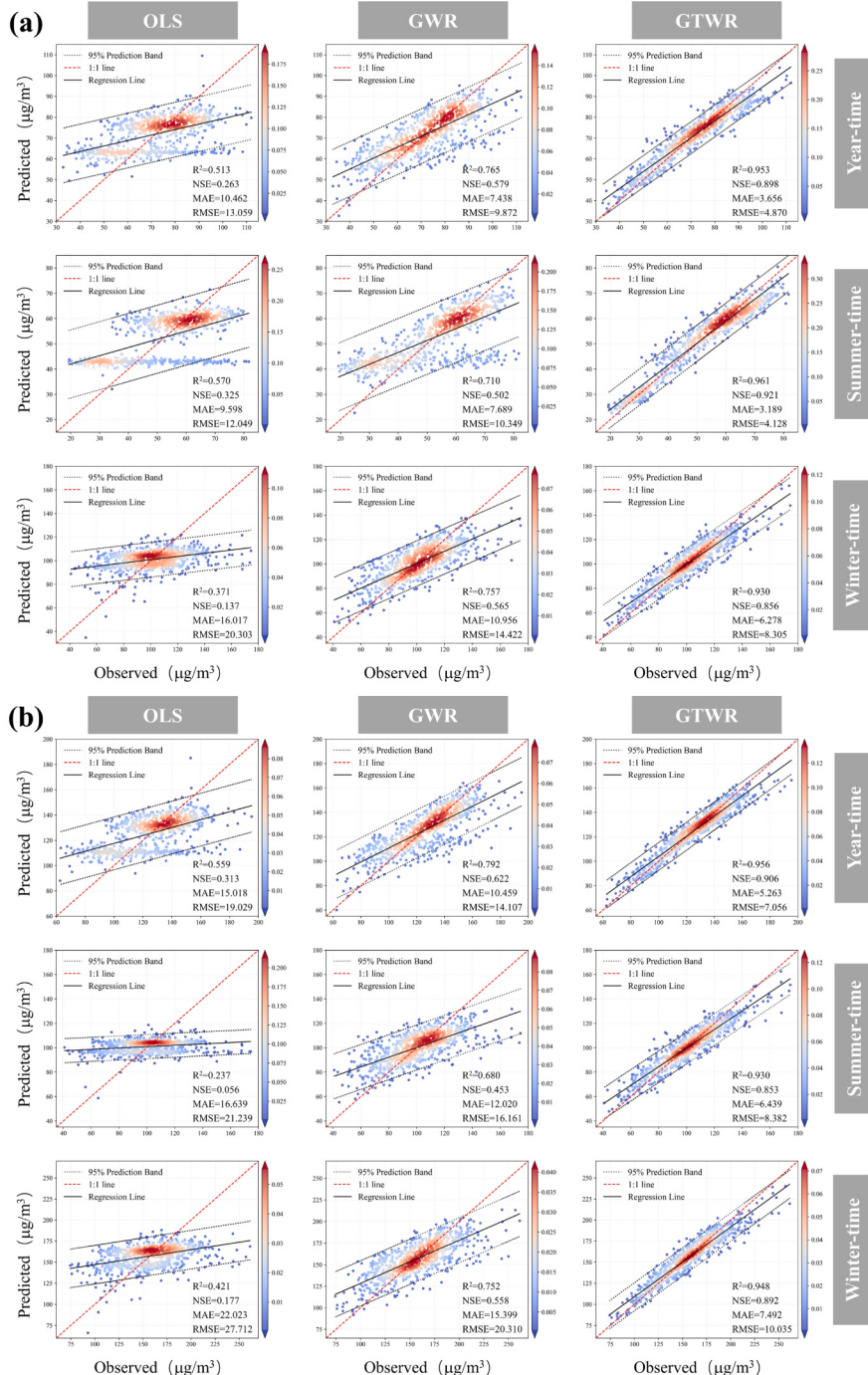


Fig. 7. Scatter plot of the relationship between LST and SUHII and PM pollution in summer and winter.

concentrations dominated. Remarkably, no areas showed a significant increase in PM<sub>2.5</sub> and PM<sub>10</sub>, indicating that the pollution prevention and control measures during the study period were effective in curbing particulate pollutants. However, it is important to note that the areas showing significant decreases in PM<sub>2.5</sub> or PM<sub>10</sub> concentrations are relatively limited. While the summer period shows a higher percentage of areas with a significant decrease (20.06 %), it still highlights the need for continued efforts in pollution prevention and control. Although the spatial distribution of PM<sub>2.5</sub> and PM<sub>10</sub> appears similar across the five sections, there are still differences in local trends. For example, while PM<sub>10</sub> concentrations in Beijing showed a significant decreasing trend in three periods, PM<sub>2.5</sub> concentrations only showed a significant decrease in summer.



**Fig. 8.** Scatter plot of OLS, GWR and GTWR model fitting results.  
(a)-PM<sub>2.5</sub>, (b)-PM<sub>10</sub>.

Then we compiled a line plot of PM<sub>2.5</sub> and PM<sub>10</sub> pollution changes from 2000 to 2021 (Fig. 5f). From a long-term perspective, the particulate pollutants concentration in the “2 + 36” cities showed an “inverted U-shaped” evolution pattern. The pollution peaks appeared in the winter of 2013, and the pollution concentrations were 140.224 µg/m<sup>3</sup> and 208.343 µg/m<sup>3</sup>, respectively. In 2021, they have dropped to 62.384 µg/m<sup>3</sup> and 110.99 µg/m<sup>3</sup>, with a decrease of about 55.51 % and 46.73 %. As far as single pollutant is concerned, the concentration of PM<sub>10</sub> fluctuated greatly, especially in winter. Because of the different pollution differences between the two, only focusing on one of them may underestimate the degree of atmospheric particulate matter pollution, resulting in inaccurate analysis of air quality.

Given the evident “inverted U-shaped” evolution pattern of PM pollution in the “2 + 36” cities, it is essential to explore how this pattern manifests in each city. Differences in economic and social development stages, as well as environmental governance measures, lead to varying inflection points and trends in pollutant concentration changes across cities. Therefore, this study used piecewise linear regression analysis to identify key inflection points in annual average, summer average, and winter average PM<sub>2.5</sub> and PM<sub>10</sub> concentrations for each city. The change in slope before and after each inflection point was also marked to clarify the different stages of PM pollution across key areas of air pollution prevention and control (Fig. S1 & S2).

Overall, the identification of inflection points reveals the non-linear temporal changes in PM pollutant concentrations, with substantial differences in trends before and after the inflection points. Therefore, the period before each city’s inflection point (including the year of the inflection point) is defined as the “increase stage” and the period after the inflection point is defined as the “decrease stage”.

### 3.4. Differences in model results at different stages at the regional scale

Understanding the stages of PM pollution development is essential for analyzing the underlying mechanisms and trends. Different stages of development may involve different mechanisms of pollution. This study conducted a comparative analysis across different stages of pollution to investigate how SUHII affects PM pollution during the various pollution stages in the “2 + 36” cities. In this study, PM<sub>2.5</sub> and PM<sub>10</sub> concentrations in cities from 2000 to 2021 were selected as the dependent variables, and SUHII and six other socio-ecological factors were used as independent variables. The OLS, GWR and GTWR models were established in the form of panel data, and the scatter plots of the predicted values and observed values of each model were drawn (Fig. 8). By comparing the R<sup>2</sup>, NSE, MAE and RMSE of each model, it was found that the GTWR model shows more reliable estimation effect and smaller prediction error than the GWR and OLS models in each period.

The analysis results of the GTWR model for PM<sub>2.5</sub> and PM<sub>10</sub> were shown in Table 2 and Fig. 9. For PM<sub>2.5</sub>, D\_SUHII generally had a negative impact on PM<sub>2.5</sub> concentrations, but this effect turned positive in the Winter-Decrease stage, which may be related to pollution sources and pollution concentration changes and special meteorological conditions (such as inversion layer). However,

**Table 2**

The model results for various development stages at the region scale.

Time	Year		Summer		Winter	
	Increase stage	Decrease stage	Increase stage	Decrease stage	Increase stage	Decrease stage
<b>PM<sub>2.5</sub> stage</b>						
Intercept	76.774	63.260	58.440	42.961	104.388	93.450
D_SUHII	-0.877	-1.128	-0.331	-0.347	-2.195	1.765
N_SUHII	0.282	0.511	-0.076	0.236	-1.721	1.136
Int_D_LST	1.047	-0.403	-0.459	-0.087	-0.605	-3.566
Int_N_LST	0.496	-0.059	0.584	-0.261	0.450	-2.141
Int_EVI	-0.284	0.310	-1.940	0.424	-3.508	-0.270
Int_PRE	-1.020	0.684	0.939	0.752	3.007	3.973
Int_POP	1.694	-0.136	2.622	-0.437	2.536	-1.820
Int_NTL	1.140	2.308	-2.246	1.060	-3.649	3.413
Diagnostic information	R <sup>2</sup> = 0.841	R <sup>2</sup> = 0.898	R <sup>2</sup> = 0.807	R <sup>2</sup> = 0.933	R <sup>2</sup> = 0.807	R <sup>2</sup> = 0.901
<b>PM<sub>10</sub> stage</b>						
Intercept	133.843	110.733	102.301	96.506	164.564	143.140
D_SUHII	-1.637	-2.667	-0.325	-1.137	-1.859	-0.873
N_SUHII	0.801	0.199	0.350	-0.141	-2.253	-0.284
Int_D_LST	1.330	0.194	-1.948	-2.737	-0.114	-5.027
Int_N_LST	0.555	-0.033	3.237	0.714	0.264	-3.199
Int_EVI	-0.404	0.637	-1.900	-1.109	-3.714	2.241
Int_PRE	-1.532	0.251	-1.185	1.049	4.640	3.504
Int_POP	2.778	0.831	4.130	0.895	2.014	-0.063
Int_NTL	1.778	3.272	-4.083	-0.036	-2.354	2.830
Diagnostic information	R <sup>2</sup> = 0.845	R <sup>2</sup> = 0.901	R <sup>2</sup> = 0.795	R <sup>2</sup> = 0.897	R <sup>2</sup> = 0.828	R <sup>2</sup> = 0.941

Here X<sub>1</sub>-X<sub>8</sub> correspond in order to the factors in Table 2.

N\_SUHII showed a negative impact in the increase stage of summer and winter, but turned positive during the rest of the periods. This suggests that, although SUHI at night may help reduce PM<sub>2.5</sub> concentrations in some periods, the stable atmosphere at night generally leads to an increase in pollutant concentration, especially in winter.

For PM<sub>10</sub>, D\_SUHII consistently exhibited a negative effect across all periods, especially during the Year-Decrease stage. This may be related to daytime thermal convection enhancing atmospheric mixing and thus reduces particle aggregation. In contrast, N\_SUHII negatively impacts PM<sub>10</sub> concentrations during winter, with the strongest effect occurring in the increase stage.

Generally, social factors may aggravate PM pollution, while ecological factors show a mitigating effect. However, the results of this study indicates that this pattern does not always hold. This may be due to the difference in the SUHI effect across different regions, influenced by factors such as geographical location, climatic conditions, urbanization process and greening levels. Int\_POP and Int\_NTL are the most significant contributors to increased PM pollution during the annual and summer. However, Int\_PRE is the most significant factor in winter. Specifically, Int\_POP has the greatest influence in the increase stage, but its influence diminishes rapidly in the decrease stage, even becoming negative. On the other hand, the influence of Int\_NTL, which is also a social factor, increased in the decline stage, indicating that the continued economic activity at night may pose a certain challenge to the emission reduction of pollutants, which may be related to the change of pollution sources caused by pollution control measures. The box plot (Fig. 9) drawn by the regression results of each city also intuitively supports this result. In the increase stage, the median of the influence of each factor is generally high and mostly positive, while in the decrease stage, the median is generally low and partially negative. In addition, the extreme value of the decrease stage and the height of the box are significantly reduced, indicating that the differences between different cities in this stage are decreasing.

It was observed that the influence of each factor changed greatly across different stages. In order to explore its changes between different stages, this study further sorted out the change of factor influence  $\Delta$  (Table 3). From the perspective of the region, the influence of D\_SUHII on PM pollution showed a downward trend except in winter. On the contrary, the influence of N\_SUHII on PM<sub>2.5</sub> increased in all periods, but the influence on PM<sub>10</sub> only increased in winter.

Among other socio-ecological factors,  $\Delta$ Int\_NTL in winter was the largest, and its  $\Delta$  on PM<sub>2.5</sub> and PM<sub>10</sub> reached 7.062 and 5.184, respectively, which proved that the impact of Int\_NTL on PM pollution is increasing as it enters the decrease stage. However, Int\_EVI and Int\_POP showed an upward and downward trend, respectively, indicating that Int\_EVI will aggravate PM pollution in the context of continuous improvement of air quality, while the influence of Int\_POP factor on PM pollution is weakening.

### 3.5. Differences in model results at different stages at the city scale

To more comprehensively analyze the impact of SUHII and socio-ecological factors under its influence on PM pollution, this study also shows the influence changes of each factor in different stages at the city scale (Fig. 10 & 11). Compared with the overall analysis of the region, the analysis at the city scale can reveal the local characteristics and details of the factor changes.

From the annual results of PM<sub>2.5</sub>, the contribution of D\_SUHII to PM<sub>2.5</sub> pollution increased in the central region, while it showed a downward trend in the northern and western mountainous areas of Henan. The situation of N\_SUHII is more complicated, but Beijing, Tianjin, Shijiazhuang, Zhengzhou and other municipalities and provincial capitals have shown an increasing trend. Among other socio-ecological factors, the contribution of Int\_PRE (74.37 %) and Int\_NTL (71.80 %) to PM<sub>2.5</sub> pollution increased in most regions, but the influence of Int\_POP in 87.19 % of cities showed a downward trend, except for the three coastal cities in the northeast. The annual

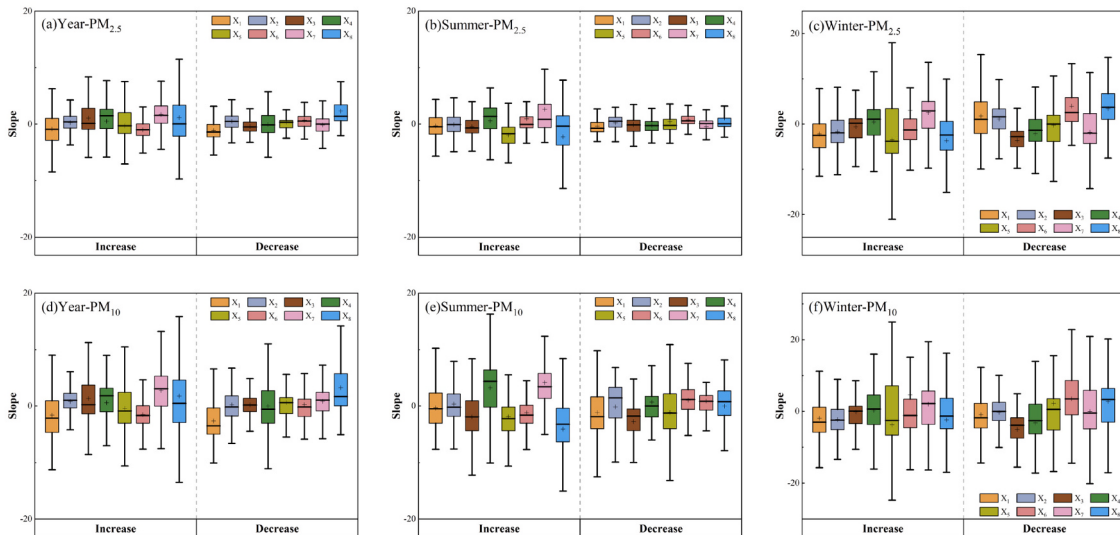


**Fig. 9.** Box plot of model results in different stages of each city.

**Table 3**

Differences in model results for different development stages at the region scale.

	PM <sub>2.5</sub>			PM <sub>10</sub>		
	Year	Summer	Winter	Year	Summer	Winter
ΔD_SUHII	-0.251	-0.016	3.960	-1.030	-0.812	0.986
ΔN_SUHII	0.229	0.312	2.857	-0.602	-0.491	1.969
ΔInt_D_LST	-1.450	0.372	-2.961	-1.136	-0.789	-4.913
ΔInt_N_LST	-0.555	-0.845	-2.591	-0.588	-2.523	-3.463
ΔInt_EVI	0.594	2.364	3.238	1.041	0.791	5.955
ΔInt_PRE	1.704	-0.187	0.966	1.783	2.234	-1.136
ΔInt_POP	-1.830	-3.059	-4.356	-1.947	-3.235	-2.077
ΔInt_NTL	1.168	3.306	7.062	1.494	4.047	5.184

Δ denotes Decrease-Increase, which is the amount of change in two stages.

results of PM<sub>10</sub> are similar, but the overall change range is large. The proportion of cities with decreasing influence of N\_SUHII and Int\_PRE is greater than PM<sub>2.5</sub>.

From the summer results of PM<sub>2.5</sub>, D\_SUHII mainly showed a trend of “decreasing in the south and increasing in the north”, while the contribution of N\_SUHII to pollution showed an increasing trend in 66.67 % of the cities, mainly distributed in the cities near 35°N and the northern cities such as Beijing and Tangshan. Among other socio-ecological factors, except for Int\_POP, the influence of most factors is increasing. In particular, Int\_N\_LST and Int\_PRE also show obvious north-south differences. The influence of Int\_POP in Beijing, Tianjin and other cities in the north has decreased significantly, and the influence of Int\_EVI in the southern cities has decreased significantly, while Int\_NTL has formed two enhancement centers in the south and north. The summer results of PM<sub>10</sub> were different from PM<sub>2.5</sub>, especially Int\_D\_LST and Int\_N\_LST. Int\_D\_LST showed an increasing trend in the northern part of the region, while Int\_N\_LST showed a completely opposite situation to PM<sub>2.5</sub> in the northern and central parts. In addition, the proportion of cities with an increasing trend of Int\_EVI influence was smaller than that of PM<sub>2.5</sub>, and the main difference of the two was Baoding-Qinhuangdao.

From the winter results of PM<sub>2.5</sub>, except for sporadic cities, the impact of SUHII on pollution is significantly enhanced, and 87.19 % of the cities in D\_SUHII show an increasing trend, especially in the eastern region showing a clear high value aggregation. However, only 4 cities in N\_SUHII showed a downward trend, with Beijing and Qinhuangdao showing the largest increase. Among other socio-ecological factors, Int\_D\_LST was quite different from other time periods, and 87.18 % of cities had a decreasing impact on PM<sub>2.5</sub>. In addition, through comparison, it can be seen that the variation range of each factor in winter is the largest in the three periods. Unlike PM<sub>2.5</sub>, the winter results of PM<sub>10</sub> indicated that D\_SUHII showed a downward trend in the west, and N\_SUHII showed a downward trend in Baoding-Cangzhou-Dongying in the north and Rizhao-Linyi-Shangqiu in the southeast. The variation pattern of Int\_POP and Int\_NTL on PM<sub>10</sub> concentration in winter is more complex, and it does not show the same trend as PM<sub>2.5</sub>.

In summary, the city-scale analysis reveals that the impact of SUHII and other socio-ecological factors in different periods and different cities has significant seasonal and regional differences. This study shows that the causes of PM pollution are diversified and dynamic in the context of continuous intensification of SUHI. Therefore, the future urban PM pollution control needs to adopt a targeted comprehensive treatment method to effectively deal with the complex pollution pattern.

#### 4. Discussion

##### 4.1. Variation trend of LST and PM pollution

The variation of LST between day and night in the study area is significantly different, which is mainly due to the difference in heat transfer mechanism between urban surface and natural surface. During the daytime, due to the lower albedo of urban impervious surfaces (such as concrete, asphalt, etc.), which can absorb more solar radiation, coupled with low evaporation capacity, the latent heat released is less, resulting in urban LST significantly higher than the surrounding natural surface. In contrast, the vegetation coverage area significantly reduces the local LST through evaporation, and the plant roots absorb soil moisture and release water vapor through transpiration, which effectively alleviates the daytime surface warming (Zhao and Zhang, 2018). At night, the impervious surface material in urban will quickly release the heat stored during the daytime, so that the nighttime LST of the urban area remains at a high level. In the natural surface area, especially near the water body, the high specific heat capacity of water makes the heat stored in the daytime release slowly, resulting in relatively high LST at night. These mechanisms explain the phenomenon of high nighttime LST in some reservoirs and coastal areas observed in the study (Tran et al., 2017; Gooseff et al., 2005). In addition, some studies have shown that the concentration changes of PM<sub>2.5</sub> and PM<sub>10</sub> are related to the variation trend of LST (Li et al., 2017). In general, higher LST during the daytime will enhance atmospheric convection and promote the vertical diffusion of particulate matter, thereby reducing the concentration of surface particulate matter. At night, due to the increase of the stability of the lower atmosphere and the formation of the inversion layer, the convection and the diffusion of particles are inhibited, resulting in an increase in the concentration of surface particles.

The results of this study indicated that the concentrations of PM<sub>2.5</sub> and PM<sub>10</sub> pollutants showed an “inverted U-shaped” trend of increasing first and then decreasing in annual, summer and winter. This trend is closely related to a series of severe pollution prevention and control measures adopted by China after the release of the “Action Plan for Air Pollution Prevention and Control” in

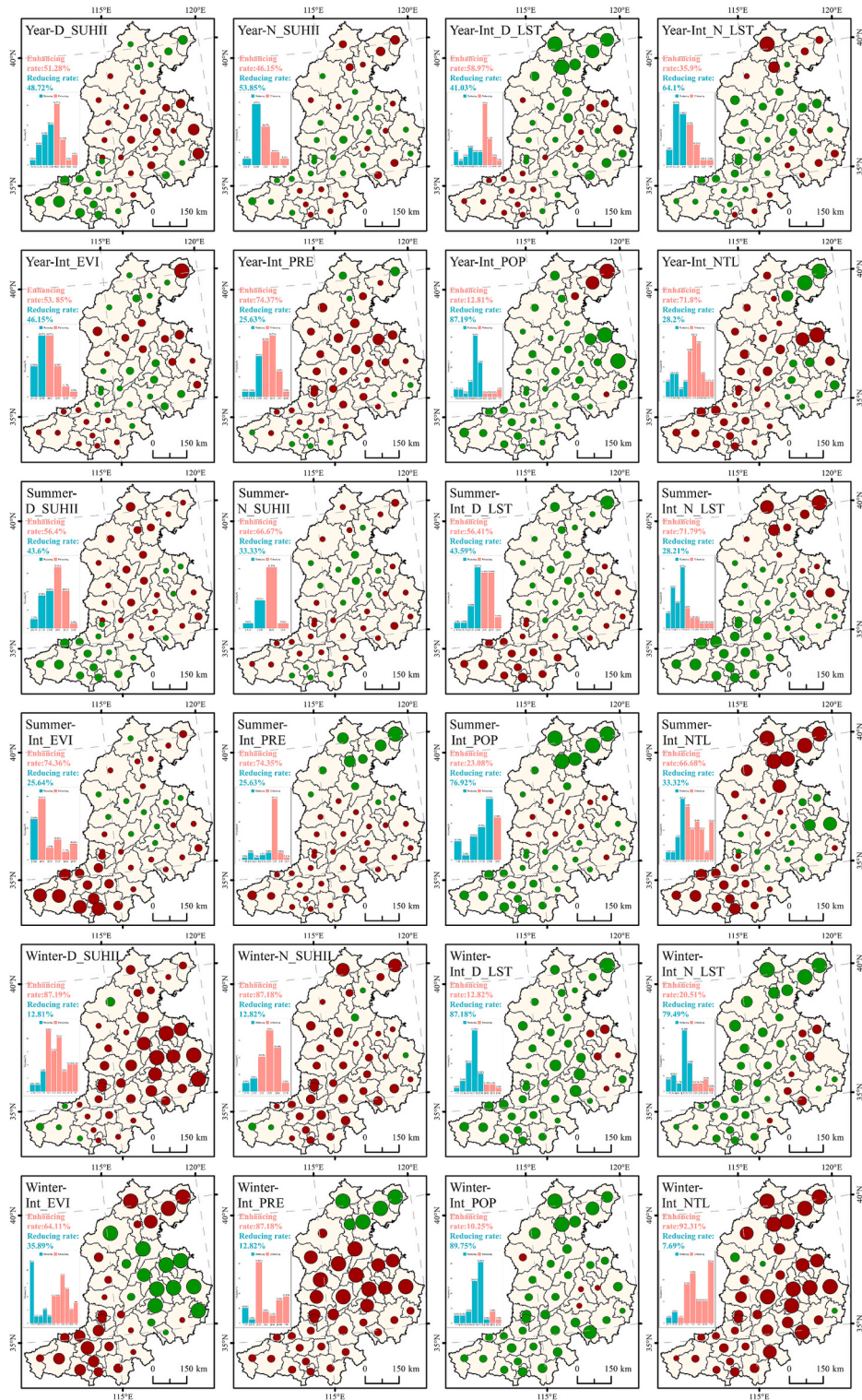


**Fig. 10.** Differences in model results under different development stages of PM<sub>2.5</sub> in different cities.

September 2013 and the “Outline of the Beijing-Tianjin-Hebei Coordinated Development Plan” in April 2015. The implementation of these measures not only significantly reduced the concentration of air pollutants in the short term, but also promoted long-term environmental improvement and continuous improvement of air quality by promoting high-quality economic development and

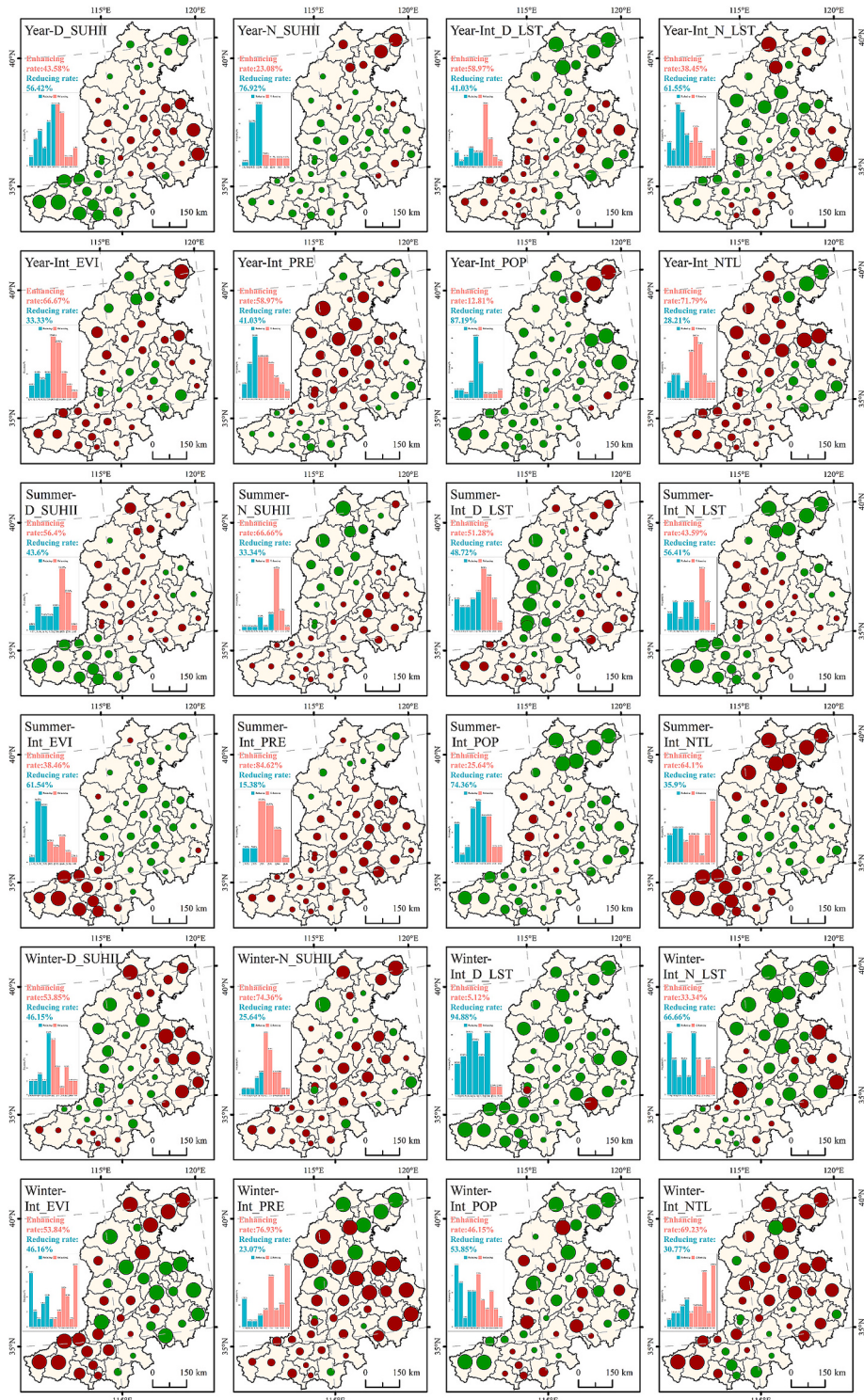


Fig. 11. Differences in model results under different development stages of PM<sub>10</sub> in different cities.

ecological protection in the region (Chang et al., 2019; Wu et al., 2020).

#### 4.2. Relationship between PM pollution and SUHI

Owing to the notable correlation between LST and PM pollution, a considerable number of studies have selected LST as one of the driving factors in the research of PM pollution drivers (Li et al., 2024; Chang et al., 2024). This is primarily due to the fact that LST can not only influence the diffusion process of pollutants by altering the stability of the atmosphere but also directly or indirectly affect the formation and transformation of pollutants through various means, thereby exerting a profound influence on the spatial and temporal distribution of pollutants (Liang et al., 2019; Ulpiani, 2021). In addition, the change of LST may also interact with other environmental parameters, which may further aggravate or alleviate pollution. It needs to be emphasised that LST data is only used to calculate the correlation between SUHII and PM concentration. The results merely indicate a trend that could be associated with underlying factors of urban morphology and meteorological conditions, rather than suggesting that UHI directly contributes to PM concentration.

In the urban environment, the abnormal phenomenon of LST is usually manifested as SUHI. This phenomenon is particularly significant in regions with rapid urbanization. The “2 + 36” cities are in line with this feature. This region covers most of the Beijing-Tianjin-Hebei urban agglomeration, the Central Plains urban agglomeration and the Shandong Peninsula urban agglomeration. They all have experienced rapid urbanization and industrialization. Cities have expanded rapidly, and the “urban disease” such as SUHI were widespread. Furthermore, this region is also a key area for air pollution prevention and control designated by the Chinese government. The air pollution situation in this region is more severe. The SUHI phenomenon in this region not only enhances the temperature disparity between urban and suburban areas but also may exacerbate the accumulation and retention of pollutants due to the special microclimate within the city, leading to a further deterioration of air quality.

Therefore, in the study of urban PM pollution, ignoring the impact of SUHI may lead to misjudgment of pollution sources and pollution diffusion mechanisms, affecting the effectiveness of pollution control measures. Especially in the context of increasing global warming, SUHI may be further intensified, which makes it particularly critical to study the relationship between SUHI and particulate matter pollution. By better understanding this relationship, researchers and policy makers can develop more accurate and effective urban air quality management strategies to cope with possible more severe pollution challenges in the future.

#### 4.3. Driver selection and comparison of two spatial scales

In addition to LST, EVI, PRE, POP, and NTL are also important influences that contribute to particulate matter pollution. EVI is used to measure the growth of vegetation, and the health of vegetation directly affects air quality and pollutant concentrations. Specifically, vegetation can reduce PM pollution by lowering air temperature and increasing ground humidity through photosynthesis (Zhang et al., 2016). Vegetation can also directly reduce airborne particulate matter through absorption and filtration. In addition, EVI is more sensitive to detecting vegetation dynamics in high biomass areas than other vegetation indices and is less susceptible to atmospheric and soil background noise, which makes it particularly suitable for monitoring vegetation cover in urban green spaces and agricultural lands (Fan et al., 2021). Rainfall, as reflected in the PRE, is an important part of the self-purification process of the atmosphere, where raindrops collide with particulate matter to form larger composites that are more likely to settle to the ground. The study of Wu (Wu et al., 2021a, 2021b) found that heavy rainfall removed more than 50 % of PM2.5 in Nanjing. Chen (Chen et al., 2018) quantitatively compared the effects of rainfall factors on PM2.5 concentrations in 188 monitored cities in China, and also verified their significant effects on PM2.5 concentrations at the national scale. Socio-economic factors such as POP and NTL are also important influences on PM pollution; high population densities are usually accompanied by high-intensity socio-economic activities, and the nighttime lighting index can directly reflect the intensity of human activities.

It is important to consider different spatial scales when studying the effects of SUHI on urban particulate pollutants at different stages. The “2 + 36” cities, as the key air pollution prevention and control region, are favored from the scale of the region as a whole, which is conducive to grasping its performance and impact on a larger scale from a macroscopic point of view. The local city scale, on the other hand, allows for a more detailed analysis of the impact of SUHI on particulate matter pollution in a given city. This has the advantage of providing a more comprehensive understanding of the relationship between SUHI and particulate matter pollution. At the overall regional scale, macro-environmental policies and plans can be formulated to coordinate the development of different areas to reduce the overall impact of heat island effect and particulate matter pollution. At the local city scale, targeted measures, such as increasing urban green space and optimizing urban layout, can be taken to mitigate the heat island effect and reduce particulate matter pollution with respect to the characteristics of specific cities. Meanwhile, by comparing the results of studies at different scales, the formation mechanisms of heat island effect and particulate matter pollution can be better understood, and the complex interaction mechanisms can be revealed to provide a basis for formulating more scientific and effective response strategies.

#### 4.4. Relevant policy recommendations derived from the results

As China enters a stage of high-quality development, the standards of atmospheric environmental protection and air pollution control are also constantly improving, and the supervision of pollution sources has also expanded from point source control to global fine management. Our research focuses on the key prevention and control areas of air pollution. In the long-term period from 2000 to 2021, we explored the differences in the impact of SUHI on PM pollutants in cities at different pollution stages from three periods of the year, summer and winter. Our research results may be of great significance in improving the ability of cities to control air pollution.

The ecological management and high-quality development of the region are inseparable from the research on SUHI and air quality.

The SUHI phenomenon is still significant in the “2 + 36” cities. N\_SUHII has a significant upward trend in three periods, and its influence on PM pollutants has increased in the decrease stage. Therefore, how to control and evacuate the heat source in the domain is a problem that needs to be focused on in the future. Large-scale human activities and industrial agglomeration are one of the main sources of urban heat, and heat source change is not unrelated to land use change (Ouyang et al., 2019; Pok et al., 2017). The increasing influence of Int\_NTL, which is closely related to land use change, also illustrates this problem. Therefore, optimizing the layout of land use and promoting regional coordination and green sustainable development can effectively reduce the accumulation of heat sources and alleviate the negative impact of SUHI on urban air quality. For example, since 2017, China has vigorously developed Xiongan New Area in Baoding, Hebei Province, as a place to relieve Beijing's non-capital functions (Wang et al., 2019). However, it cannot be ignored that other cities may be difficult to make similar corresponding changes through policy implementation in a short period of time. Therefore, policy makers should fully consider the current situation of the region and improve the regional thermal environment through industrial transformation or technological upgrading. In general, in recent years, due to the further implementation of air pollution prevention measures and regional collaborative governance, the concentration of PM pollutants in the region has been greatly reduced. However, to further improve the quality of regional development, government decision makers should take the initiative to adjust the planning objectives and increase policy support for their own resource-poor areas and other cities in the region.

## 5. Conclusion

Although the impact of LST on air quality has been demonstrated, the microclimate changes caused by built-up areas, especially the spatial transfer of SUHI and PM pollutants, still lack in-depth research. This study reveals the spatial and temporal evolution characteristics and trend differentiation of LST and PM pollutants in the “2 + 36” cities, which are the key prevention and control areas of air pollution, from 2000 to 2021. The inflection points of pollution in each period are identified by quantitative means, and the influence of SUHII and its socio-ecological factors on PM pollutants at different stages is further discussed. It was found that SUHI was ubiquitous in the region, and N\_SUHII increased significantly. It is further found that the impact of N\_SUHII and Int\_NTL on PM pollution in many cities has been greatly increased, reflecting the unique position of current night activities in the pollution mechanism. Of course, there are seasonal and regional differences in the impact of SUHII on PM pollution. To break through the “platform period” of current pollution control, targeted control measures should be further taken according to their own characteristics.

City is an important carrier of modernization. This study deepens the understanding of the transmission mechanism of air pollutants, and further confirms the important role of collaborative control theory in the process of air pollution prevention and control, which can provide reference for other developing countries with similar development process. However, it should be admitted that due to the complexity of the urban environment, it is difficult to fully characterize the impact of SUHII on PM pollution in a long time series through the existing data in this study. For example, the lack of accuracy of the remote sensing dataset will inevitably lead to the error of the research results. Therefore, in order to further explore the relationship between urban microclimate and PM pollution, we will use higher-precision and larger-scale datasets for deeper analysis in the future to contribute to the sustainable development of the city.

## CRediT authorship contribution statement

**Chang Yinghui:** Writing – original draft, Software, Formal analysis, Data curation. **Guo Xiaomin:** Writing – review & editing, Supervision, Funding acquisition, Conceptualization.

## Declaration of competing interest

The authors declare that they have no known competing financial interests or personal relationships that could have appeared to influence the work reported in this paper.

## Data availability

Data will be made available on request.

## Appendix A. Supplementary data

Supplementary data to this article can be found online at <https://doi.org/10.1016/j.ulclim.2024.102273>.

## References

- Cao, S.P., Zhang, L.F., He, Y., Zhang, Y.L., Chen, Y., Yao, S., Yang, W., Sun, Q., 2022. Effects and contributions of meteorological drought on agricultural drought under different climatic zones and vegetation types in Northwest China. *Sci. Total Environ.* 821, 153270. <https://doi.org/10.1016/j.scitotenv.2022.153270>.  
 Cao, S.P., He, Y., Zhang, L.F., Sun, Q., Zhang, Y.L., Li, H.Z., Wei, X., Liu, Y.X., 2023. Spatiotemporal dynamics of vegetation net ecosystem productivity and its response to drought in Northwest China. *GISci. Remote Sens.* 60 (1), 2194597. <https://doi.org/10.1080/15481603.2023.2194597>.

- Chang, X., Wang, S.X., Zhao, B., Xing, J., Liu, X.X., Wei, L., Song, Y., Wu, W.J., Cai, S.Y., Zheng, H.T., Ding, D., Zheng, M., 2019. Contributions of inter-city and regional transport to PM<sub>2.5</sub> concentrations in the Beijing-Tianjin-Hebei region and its implications on regional joint air pollution control. *Sci. Total Environ.* 660, 1191–1200. <https://doi.org/10.1016/j.scitotenv.2018.12.474>.
- Chang, Y.H., Li, G.H., Zhang, P.Y., Liu, Y., Chen, Z., Xing, G.R., Li, M.F., 2024. Relationships among six urban air pollutants and identification of pollution types – a case study of Chinese cities above prefecture level. *Atmos. Pollut. Res.* 15, 102160. <https://doi.org/10.1016/j.apr.2024.102160>.
- Chen, B., Kong, F.H., Meadows, M.E., Pan, H.J., Zhu, A.X., Chen, L.D., Yin, H.W., Yang, L., 2024a. The evolution of social-ecological system interactions and their impact on the urban thermal environment. *npj Urban Sustain.* 4, 3. <https://doi.org/10.1038/s42949-024-00141-4>.
- Chen, M.X., Liu, W.D., Tao, X.L., 2013. Evolution and assessment on China's urbanization 1960–2010: under-urbanization or over-urbanization? *Habitat Int.* 38, 25–33. <https://doi.org/10.1016/j.habitatint.2012.09.007>.
- Chen, Y.L., Rich, D.Q., Hopke, P.K., 2024b. Changes in source specific PM<sub>2.5</sub> from 2010 to 2019 in New York and New Jersey identified by dispersion normalized PMF. *Atmos. Res.* 304, 107353. <https://doi.org/10.1016/j.atmosres.2024.107353>.
- Chen, Z.Y., Xie, X.M., Cai, J., Chen, D.L., Gao, B.B., He, B., Cheng, N.L., Xu, B., 2018. Understanding meteorological influences on PM<sub>2.5</sub> concentrations across China: a temporal and spatial perspective. *Atmos. Chem. Phys.* 18, 5343–5358. <https://doi.org/10.5194/acp-18-5343-2018>.
- Estoque, R.C., Ooba, M., Seposo, X.T., Togawa, T., Hijioka, Y., Takahashi, K., Nakamura, S., 2020a. Heat health risk assessment in Philippine cities using remotely sensed data and social-ecological indicators. *Nat. Commun.* 11, 1–12. <https://doi.org/10.1038/s41467-020-15218-8>.
- Estoque, R.C., Ooba, M., Seposo, X.T., Togawa, T., Hijioka, Y., Takahashi, K., Nakamura, S., 2020b. Heat health risk assessment in Philippine cities using remotely sensed data and social-ecological indicators. *Nat. Commun.* 11, 1581. <https://doi.org/10.1038/s41467-020-15218-8>.
- Fan, X., Song, Y.Z., Zhu, C.X., Balzter, H., Bai, Z.K., 2021. Estimating ecological responses to climatic variability on reclaimed and unmined lands using enhanced vegetation index. *Remote Sens.* 13, 1100. <https://doi.org/10.3390/rs13061100>.
- Funk, C., Peterson, P., Landsfeld, M., Pedreros, D., Verdini, J., Shukla, S., Husak, G., Rowland, J., Harrison, L., Hoell, A., Michaelsen, J., 2015. The climate hazards infrared precipitation with stations—a new environmental record for monitoring extremes. *Sci. Data.* 2, 150066. <https://doi.org/10.1038/sdata.2015.66>.
- Geng, G.N., Xiao, Q.Y., Zheng, Y.X., Tong, D., Zhang, Y.X., Zhang, X.Y., Zhang, Q., He, K.B., Liu, Y., 2019. Impact of China's air pollution prevention and control action plan on PM<sub>2.5</sub> chemical composition over eastern China. *Sci. China Earth Sci.* 62, 1872–1884. <https://doi.org/10.1007/s11430-018-9353-x>.
- Giovannini, L., Ferrero, E., Karl, T., Rotach, M.W., Staquet, C., Castelli, S.T., Zardi, D., 2020. Atmospheric pollutant dispersion over complex terrain: challenges and needs for improving air quality measurements and modeling. *Atmosphere* 11 (6), 646. <https://doi.org/10.3390/atmos11060646>.
- Gooseff, M.N., Strzepek, K., Chapra, S.C., 2005. Modeling the potential effects of climate change on water temperature downstream of a shallow reservoir, lower Madison river. *MT. Climatic Change* 68, 331–353. <https://doi.org/10.1007/s10584-005-9076-0>.
- Grimm, N.B., Faeth, S.H., Golubiewski, N.E., Redman, C.L., Wu, J., Bai, X., Briggs, J.M., 2008. Global change and the ecology of cities. *Science* 319, 756–760. <https://doi.org/10.1126/science.1150195>.
- Huang, B., Wu, B., Barry, M., 2008. Geographically and temporally weighted regression for modeling spatio-temporal variation in house prices. *Int. J. Geogr. Inf. Sci.* 24, 383–401. <https://doi.org/10.1080/13658810802672469>.
- Jiang, Y.Y., Xin, J.Y., Wang, Y., Tang, G.Q., Zhao, Y.X., Jia, D.J., Zhao, D.D., Wang, M., Dai, L.D., Wang, L.L., Wen, T.X., Wu, F.K., 2021. The thermodynamic structures of the planetary boundary layer dominated by synoptic circulations and the regular effect on air pollution in Beijing. *Atmos. Chem. Phys.* 21, 6111–6128. <https://doi.org/10.5194/acp-21-6111-2021>.
- Kolokotroni, M., Giannitsaris, I., Watkins, R., 2006. The effect of the London urban heat island on building summer cooling demand and night ventilation strategies. *Sol. Energy* 80, 383–392. <https://doi.org/10.1016/j.solener.2005.03.010>.
- Lai, L.W., Cheng, W.L., 2009. Air quality influenced by urban heat island coupled with synoptic weather patterns. *Sci. Total Environ.* 407, 2724–2733. <https://doi.org/10.1016/j.scitotenv.2008.12.002>.
- Li, S.S., Wei, G.E., Liu, Y.B., Bai, L., 2023. Multi-scale analysis of PM<sub>2.5</sub> concentrations in the Yangtze River Economic Belt: investigating the combined impact of natural and human factors. *Remote Sens.* 15 (13), 3356. <https://doi.org/10.3390/rs15133356>.
- Li, X.L., Ma, Y.J., Wang, Y.F., Liu, N.W., Hong, Y., 2017. Temporal and spatial analyses of particulate matter (PM<sub>10</sub> and PM<sub>2.5</sub>) and its relationship with meteorological parameters over an urban city in Northeast China. *Atmos. Res.* 198, 185–193. <https://doi.org/10.1016/j.atmosres.2017.08.023>.
- Li, Z., Wu, W., Chen, S.F., Zhang, Y.L., Tian, S.Q., Li, L.J., Zhao, X.G., 2024. A multi-scale analysis of the relationship between land surface temperature and PM<sub>2.5</sub> in different land use types, 15, 142980. <https://doi.org/10.1016/j.jclepro.2024.142980>.
- Liang, L.W., Wang, Z.B., Li, J.X., 2019. The effect of urbanization on environmental pollution in rapidly developing urban agglomerations. *J. Clean. Prod.* 237, 117649. <https://doi.org/10.1016/j.jclepro.2019.117649>.
- Lin, Y., Wang, Z.F., Jim, C.Y., Li, J.B., Deng, J.S., Liu, J.G., 2020. Water as an urban heat sink: blue infrastructure alleviates urban heat island effect in mega-city agglomeration. *J. Clean. Prod.* 262, 121411. <https://doi.org/10.1016/j.jclepro.2020.121411>.
- Liu, H.M., Huang, B., Gao, S.H., Wang, J., Yang, C., Li, R.R., 2021. Impacts of the evolving urban development on intra-urban surface thermal environment: evidence from 323 Chinese cities. *Sci. Total Environ.* 771, 144810. <https://doi.org/10.1016/j.scitotenv.2020.144810>.
- Liu, Z.H., Zhan, W.F., Bechtel, B., Voogt, J., Lai, J.M., Chakraborty, T., Wang, Z.H., Li, M.C., Huang, F., Lee, X.H., 2022. Surface warming in global cities is substantially more rapid than in rural background areas. *Commun. Earth Environ.* 3, 219. <https://doi.org/10.1038/s43247-022-00539-x>.
- Luo, H., Han, Y., Lu, C.S., Yang, J., Wu, Y.H., 2019. Characteristics of surface solar radiation under different air pollution conditions over Nanjing, China: observation and simulation. *Adv. Atmos. Sci.* 36, 1047–1059. <https://doi.org/10.1007/s00376-019-9010-4>.
- Mackey, C.W., Lee, X.H., Smith, R.B., 2012. Remotely sensing the cooling effects of city scale efforts to reduce urban heat island. *Build. Environ.* 49, 348–358. <https://doi.org/10.1016/j.buildenv.2011.08.004>.
- Martin Patience, 2013. Beijing Smog: When Growth Trumps Life in China, BBC, Beijing. [www.bbc.co.uk/news/magazine21198265](http://www.bbc.co.uk/news/magazine21198265).
- Meehl, G.A., Tebaldi, C., 2004. More intense, more frequent, and longer lasting heat waves in the 21st century. *Science* 305, 994–997.
- Ngarambe, J., Joen, S.J., Han, C.H., Yun, G.Y., 2021. Exploring the relationship between particulate matter, CO, SO<sub>2</sub>, NO<sub>2</sub>, O<sub>3</sub> and urban heat island in Seoul, Korea. *J. Hazard. Mater.* 403, 123615. <https://doi.org/10.1016/j.jhazmat.2020.123615>.
- Ouyang, Z.T., Lin, M.M., Chen, J.Q., Fan, P.L., Qian, S.S., Park, H., 2019. Improving estimates of built-up area from night time light across globally distributed cities through hierarchical modeling. *Sci. Total Environ.* 647, 1266–1280. <https://doi.org/10.1016/j.scitotenv.2018.08.015>.
- Peng, S.S., Piao, S.L., Ciais, P., Friedlingstein, P., Ottles, C., Bréon, F.-M., Nan, H.J., Zhou, L.M., Myneni, R.B., 2012. Surface urban heat island across 419 global big cities. *Environ. Sci. Technol.* 46, 696–703. <https://doi.org/10.1021/es2030438>.
- Pok, S., Matsushita, B., Fukushima, T., 2017. An easily implemented method to estimate impervious surface area on a large scale from MODIS time-series and improved DMSP-OLS nightime light data. *ISPRS J. Photogramm. Remote Sens.* 133, 104–115. <https://doi.org/10.1016/j.isprsjprs.2017.10.005>.
- Qi, J., Zheng, B., Li, M., Yu, F., Chen, C.C., Liu, F., Zhou, X.F., Yuan, J., Zhang, Q., He, K.B., 2017. A high-resolution air pollutants emission inventory in 2013 for the Beijing-Tianjin-Hebei region, China. *Atmos. Environ.* 170, 156–168. <https://doi.org/10.1016/j.atmosenv.2017.09.039>.
- Santamouris, M., 2020. Recent progress on urban overheating and heat island research. Integrated assessment of the energy, environmental, vulnerability and health impact. Synergies with the global climate change. *Energ. Build.* 207, 109482. <https://doi.org/10.1016/j.enbuild.2019.109482>.
- Sarrat, C., Lemonas, A., Masson, V., Guedalia, D., 2006. Impact of urban heat island on regional atmospheric pollution. *Atmos. Environ.* 40, 1743–1758. <https://doi.org/10.1016/j.atmosenv.2005.11.037>.
- Tian, S.L., Pan, Y.P., Liu, Z.R., Wen, T.X., Wang, Y.S., 2014. Size-resolved aerosol chemical analysis of extreme haze pollution events during early 2013 in urban Beijing, China. *J. Hazard. Mater.* 279, 452–460. <https://doi.org/10.1016/j.jhazmat.2014.07.023>.
- Tie, X.X., Huang, R.J., Cao, J.J., Zhang, Q., Cheng, Y.F., Su, H., Chang, D., Pöschl, U., Hoffmann, T., Dusek, U., Li, G.H., Worsnop, D.R., O'Dowd, C.D., 2017. Severe pollution in China amplified by atmospheric moisture. *Sci. Rep.* 7, 15760. <https://doi.org/10.1038/s41598-017-15909-1>.
- Tran, D.X., Pla, F., Latorre-Carmona, P., Myint, S.W., Caetano, M., Kieu, H.V., 2017. Characterizing the relationship between land use land cover change and land surface temperature. *ISPRS J. Photogramm.* 124, 119–132. <https://doi.org/10.1016/j.isprsjprs.2017.01.001>.

- Ulpiani, G., 2021. On the linkage between urban heat island and urban pollution island: three-decade literature review towards a conceptual framework. *Sci. Total Environ.* 751, 141727. <https://doi.org/10.1016/j.scitotenv.2020.141727>.
- Voogt, J.A., Oke, T.R., 2003. Thermal remote sensing of urban climates. *Remote Sens. Environ.* 86, 370–384. [https://doi.org/10.1016/S0034-4257\(03\)00079-8](https://doi.org/10.1016/S0034-4257(03)00079-8).
- Wang, Y.G., Ying, Q., Hu, J.L., Zhang, H.L., 2014. Spatial and temporal variations of six criteria air pollutants in 31 provincial capital cities in China during 2013–2014. *Environ. Int.* 73, 413–422. <https://doi.org/10.1016/j.envint.2014.08.016>.
- Wang, Y.Y., Du, H.Y., Xu, Y.Q., Lu, D.B., Wang, X.Y., Guo, Z.Y., 2018. Temporal and spatial variation relationship and influence factors on surface urban heat island and ozone pollution in the Yangtze River Delta, China. *Sci. Total Environ.* 631–632, 921–933.
- Wang, Z.B., Liang, L.W., Sun, Z., Wang, X.M., 2019. Spatiotemporal differentiation and the factors influencing urbanization and ecological environment synergistic effects within the Beijing-Tianjin-Hebei urban agglomeration. *J. Environ. Manag.* 243, 227–239. <https://doi.org/10.1016/j.jenvman.2019.04.088>.
- Wei, J., Li, Z., 2023a. ChinaHighPM2.5: High-resolution and High-quality Ground-level PM2.5 Dataset for China (2000–2022). National Tibetan Plateau/Third Pole Environment Data Center. <https://doi.org/10.5281/zenodo.3539349>.
- Wei, J., Li, Z., 2023b. ChinaHighPM10: High-resolution and High-quality Ground-level PM10 Dataset for China (2000–2022). National Tibetan Plateau / Third Pole Environment Data Center. <https://doi.org/10.5281/zenodo.3752465>.
- Wu, S.S., Wang, Z.Y., Du, Z.H., Huang, B., Zhang, F., Liu, R.Y., 2021a. Geographically and temporally neural network weighted regression for modeling spatiotemporal non-stationary relationships. *Int. J. Geogr. Inf. Sci.* 35, 582–608. <https://doi.org/10.1080/13658816.2020.1775836>.
- Wu, T.C., Xie, X., Xue, B., Liu, T., 2021b. A quantitative modeling and prediction method for sustained rainfall-PM2.5 removal modes on a Micro-temporal scale. *Sustainability* 13, 11022. <https://doi.org/10.3390/su131911022>.
- Wu, Y.N., Liao, M.J., Hu, M.Y., Xu, C.B., Tao, Y., Zhou, J.L., 2020. Effectiveness assessment of air pollution prevention and control under collaborative supervision in the Beijing-Tianjin-Hebei region based on combination weights and grey fuzzy synthetic evaluation analysis. *Sustain. Cities Soc.* 64, 102543. <https://doi.org/10.1016/j.scs.2020.102543>.
- Yang, G.W., Ren, G.Y., Zhang, P.F., Xue, X.Y., Tysa, S.K., Jia, W.Q., Qin, Y., Zheng, X., Zhang, S.Q., 2021. PM2.5 influence on urban Heat Island (UHI) effect in Beijing and the possible mechanisms. *J. Geophys. Res.-Atmos.* 126, e2021JD035227. <https://doi.org/10.1029/2021JD035227>.
- Yang, J., Huang, X., 2021. The 30 m annual land cover dataset and its dynamics in China from 1990 to 2019. *Earth Syst. Sci. Data.* 13, 3907–3925. <https://doi.org/10.5194/essd-13-3907-2021>.
- Yu, Z.W., Zhang, J.G., Yang, G.Y., 2021. How to build a heat network to alleviate surface heat island effect? *Sustain. Cities Soc.* 74, 103135. <https://doi.org/10.1016/j.scs.2021.103135>.
- Zeng, Y.Y., Cao, Y.F., Qiao, X., Seyler, B.C., Tang, Y., 2019. Air pollution reduction in China: recent success but great challenge for the future. *Sci. Total Environ.* 663, 329–337. <https://doi.org/10.1016/j.scitotenv.2019.01.262>.
- Zhang, L.F., Yan, H.W., He, Y., Yao, S., Cao, S.P., Sun, Q., 2022. Spatiotemporal prediction of alpine vegetation dynamic change based on a ConvGRU neural network model: a case study of the upper Heihe River basin in Northwest China. *IEEE J-STARS.* 15, 6957–6971. <https://doi.org/10.1109/JSTARS.2022.3200521>.
- Zhang, R.H., Li, Q., Zhang, R.N., 2014. Meteorological conditions for the persistent severe fog and haze event over eastern China in January 2013. *Sci. China Earth Sci.* 57, 26–35.
- Zhang, T.H., Gong, W., Wang, W., Ji, Y.X., Zhu, Z.M., Huang, Y.S., 2016. Ground level PM2.5 estimates over China using satellite-based geographically weighted regression (GWR)models are improved by including NO<sub>2</sub> and enhanced vegetation index (EVI). *Int. J. Environ. Res. Public Health* 13, 1215. <https://doi.org/10.3390/ijerph13121215>.
- Zhao, C., Wang, B., 2022. How does new-type urbanization affect air pollution? Empirical evidence based on spatial spillover effect and spatial Durbin model. *Environ. Int.* 165, 107304. <https://doi.org/10.1016/j.envint.2022.107304>.
- Zhao, C.Y., Zhu, H.K., Zhang, S.Y., Jin, Z.W., Zhang, Y.W., Wang, Y.W., Shi, Y.D., Jiang, J.H., Chen, X.Y., Liu, M., 2024. Long-term trends in surface thermal environment and its potential drivers along the urban development gradients in rapidly urbanizing regions of China. *Sustain. Cities Soc.* 105, 105324. <https://doi.org/10.1016/j.scs.2024.105324>.
- Zhao, P.J., Zhang, M.Z., 2018. The impact of urbanisation on energy consumption: a 30-year review in China. *Urban Clim.* 24, 940–953. <https://doi.org/10.1016/j.uclim.2017.11.005>.
- Zhou, D.C., Zhao, S.Q., Zhang, L.X., Sun, G., Liu, Y.Q., 2015. The footprint of urban heat island effect in China. *Sci. Rep-UK.* 5, 11160. <https://doi.org/10.1038/srep11160>.
- Zhou, J., Zhang, X., Tang, W., Ding, L., Ma, J., Zhang, X., 2021. Daily 1-km all-Weather Land Surface Temperature Dataset for the China's Landmass and its Surrounding Areas (TRIMS LST; 2000–2022). National Tibetan Plateau / Third Pole Environment Data Center. <https://doi.org/10.11888/Meteoro.tpdc.271252>.
- Zhu, W.H., Xu, X.D., Zheng, J., Yan, P., Wang, Y.J., Cai, W.Y., 2018. The characteristics of abnormal wintertime pollution events in the Jing-Jin-Ji region and its relationships with meteorological factors. *Sci. Total Environ.* 626, 887–898. <https://doi.org/10.1016/j.scitotenv.2018.01.083>.